

FEM-Analysis of Nonclassical Transmission Conditions between Elastic Structures

Part 1: Soft Imperfect Interface.

G. Mishuris¹, A. Öchsner² and G. Kuhn³

Abstract: FEM-evaluation of imperfect transmission conditions has been performed for a modelling problem of an elastic structure with a thin intermediate interface. Very good correlations with theoretical results have been obtained. Additionally, the possible error connected with introducing the transmission conditions instead of the intermediate zone has been estimated depending on mechanical properties of the zone.

keyword: Elasticity, imperfect interface, nonclassical transmission conditions, finite element method

1 Introduction

Composite materials are usually considered as nonhomogeneous solids with perfect bonding between different phases of the composites [Allen(1969) and Ashby, Fleck, Gibson, Hutchinson, and Wadley (2000)]. On the other hand, such structures, in fact, contain thin intermediate layers matching materials of the phases together. Moreover, features of the layers may play an important role and influence the composite properties. However, when a structure consists of components of essentially different sizes and properties, FEM analysis of the structure becomes very difficult. This fact follows from the necessity to construct a complicated mesh structure which, in turn, may lead to unstable numerical calculations [Hatheyway (1989)].

The aim of this paper is to investigate by FEM analysis one of the possible approaches to avoid such problems. Namely, we are going to consider in detail the so-called imperfect interface approach. It consists of replacing the real thin interphase which is connecting the different materials by special transmission conditions. These conditions are accurately extracted by asymptotic analysis taking into account possible small parameters involved in the problem. Such a small parameter is definitely

here the thickness of the interphase between the materials. However, other parameter can also appear which are connected with the relative difference in the mechanical properties of the interphase and the bonded materials. Three cases can be separated: i.e. the soft interphase, the stiff interphase and a comparable interphase with respect to mechanical properties. The main efforts are made in the paper to verify the accuracy of the transmission conditions not in terms of the asymptotic analysis estimate (like $O(\varepsilon)$), but in exact values.

In the next section, we accurately discuss the asymptotic procedure to evaluate the transmission conditions for the soft inhomogeneous interface. In the case of the interphase with properties comparable to those of the matched materials, we refer the prospective reader to the monograph [Movchan and Movhan (1995)]. We verify the applicability of the obtained conditions and discuss edge effects appearing in the problem. Various combinations of the material parameters are under consideration. In this paper, we restrict ourselves to simple load cases and symmetrical samples for homogeneous and nonhomogeneous interphases. Stiff interphases and other effects (nonsymmetric samples, complicated loadings, norm estimates) will be investigated in the second part of the paper.

2 Asymptotic evaluation of transmission conditions between elastic bodies for soft interphase (2D-problem)

Let us consider a model plane strain problem for a bimaterial elastic solid in the rectangle $\Omega_h = \Omega_+ \cup \Omega_- \cup \Omega$, where $\Omega_{\pm} = \{(x, y), \pm y \geq h\}$, $\Omega = \{(x, y), |y| \leq h\}$ (see Fig. 1). We assume that the intermediate layer Ω is inhomogeneous and isotropic, while the bonded materials are isotropic and homogeneous.

Let $\mathbf{u}_{\pm}(x, y)$ and $\mathbf{u}(x, y)$ be vectors of displacements: $\mathbf{u}_{\pm} = [u_x^{\pm}, u_y^{\pm}]^T$, $\mathbf{u} = [u_x, u_y]^T$. They satisfy Lamé equa-

¹ RzUT, Rzeszow, POLAND.

² UA, Aveiro, PORTUGAL.

³ FAU, Erlangen, GERMANY.

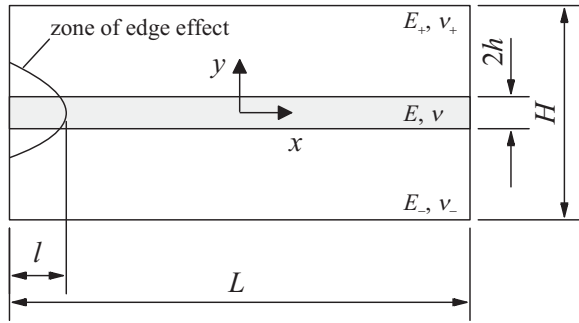


Figure 1 : Schematic representation of the problem

tions in the corresponding domains:

$$\mathcal{L}_{\pm} \mathbf{u}_{\pm} = \mathbf{0}, \quad (x, y) \in \Omega_{\pm}, \quad \mathcal{L} \mathbf{u} = \mathbf{0}, \quad (x, y) \in \Omega, \quad (1)$$

where the differential operators \mathcal{L}_{\pm} and \mathcal{L} are defined in the following manner:

$$\mathcal{L}_{\pm} = \begin{pmatrix} (\lambda_{\pm} + 2\mu_{\pm})D_x^2 + \mu_{\pm}D_y^2 & (\lambda_{\pm} + \mu_{\pm})D_x D_y \\ (\lambda_{\pm} + \mu_{\pm})D_x D_y & (\lambda_{\pm} + 2\mu_{\pm})D_y^2 + \mu_{\pm}D_x^2 \end{pmatrix}, \quad (2)$$

$$\mathcal{L} = \begin{pmatrix} D_x(\lambda + 2\mu)D_x + D_y\mu D_y & D_x\lambda D_y + D_y\mu D_x \\ D_y\lambda D_x + D_x\mu D_y & D_y(\lambda + 2\mu)D_y + D_x\mu D_x \end{pmatrix}. \quad (3)$$

Here D_x and D_y are the respective partial derivatives, while the material parameters can change their values within the interphase:

$$\mu = \mu(x, y), \quad \lambda = \lambda(x, y). \quad (4)$$

Some boundary conditions are assumed to be satisfied on the exterior boundaries:

$$\begin{aligned} \mathcal{B}_{\pm} \mathbf{u}_{\pm} &= \mathbf{0}, \quad (x, y) \in \partial\Omega_h \cap \partial\Omega_{\pm}, \\ \mathcal{B} \mathbf{u} &= \mathbf{0}, \quad (x, y) \in \partial\Omega_h \cap \partial\Omega. \end{aligned} \quad (5)$$

We do not use precise forms of the boundary operators \mathcal{B}_{\pm} and \mathcal{B} because they will not play any role in a formal asymptotic procedure. However, they are extremely important, of course, for justification of the final asymptotic estimate for the obtained solution.

Along the interior boundaries $y = \pm h$, the perfect transmission conditions (6) should be satisfied (the vectors of displacements and stresses are continuous across the interface):

$$\mathbf{u}_{\pm}(x, \pm h) = \mathbf{u}(x, \pm h), \quad \boldsymbol{\sigma}_{\pm}^{(y)}(x, \pm h) = \boldsymbol{\sigma}^{(y)}(x, \pm h), \quad (6)$$

where $\boldsymbol{\sigma}_{\pm}^{(y)}(x, \pm h)$ and $\boldsymbol{\sigma}^{(y)}(x, \pm h)$ are tractions along the boundaries of the thin interphase between the adherends which are calculated from Hooke's law:

$$\boldsymbol{\sigma}_{\pm}^{(y)}(x, y) = \mathcal{M}_{\pm} \mathbf{u}_{\pm}(x, y), \quad \boldsymbol{\sigma}^{(y)}(x, y) = \mathcal{M} \mathbf{u}(x, y), \quad (7)$$

$$\mathcal{M} = \begin{pmatrix} \mu D_y & \mu D_x \\ \lambda D_x & (\lambda + 2\mu) D_y \end{pmatrix}, \quad (8)$$

and \mathcal{M}_{\pm} are defined in the same manner by replacing μ and λ with μ_{\pm} and λ_{\pm} .

We assume that the intermediate layer is essentially thinner in comparison to the characteristic size of the body: $h \ll \min\{L, H\}$. This allows us to introduce in the problem a small dimensionless parameter $\varepsilon \ll 1$ in the following manner: $(x, y) \in \Omega$

$$y = \varepsilon \xi, \quad \xi \in [-h_0, h_0], \quad h_0 \sim \min\{L, H\}. \quad (9)$$

This makes it possible to use asymptotic methods to perform an analysis of the problem. It is a well known fact that the perfect transmission conditions are still applicable if the elastic constants of the intermediate layer are comparable in values with those of the matched materials (see, for example, [Movchan and Movhan (1995)]).

We assume in this paper that there is a significant difference in the elastic properties. Namely, there exists an additional small parameter connected with the mechanical properties of the bimaterial structure (the interphase is essentially softer than the both matched materials):

$$\mu(x, y) = \varepsilon \mu_0(x, \xi), \quad \lambda(x, y) = \varepsilon \lambda_0(x, \xi), \quad (10)$$

$$\mu_0 \sim \lambda_0, \quad \mu_0 \sim \mu_{\pm}. \quad (11)$$

Let us denote by $\mathbf{w}(x, \xi) = \mathbf{u}(x, \varepsilon \xi)$ the solution within the domain $\Omega_0 = \{(x, \xi), |\xi| \leq h_0\}$. In the new notations, all operators can be rewritten as follows:

$$\mathcal{L} = \varepsilon^{-1} \mathcal{L}_0 + \mathcal{L}_1 + \varepsilon \mathcal{L}_2, \quad \mathcal{M} = \mathcal{M}_0 + \varepsilon \mathcal{M}_1, \quad (12)$$

where $\mathcal{L}_0 = D_{\xi} \mathbf{A}_0 D_{\xi}$, $\mathcal{L}_2 = D_x \mathbf{A}_2 D_x$, $\mathcal{M}_0 = \mathbf{A}_0 D_{\xi}$, $\mathcal{M}_1 = \mathbf{A}_1 D_x$, $\mathbf{A}_0 \mathbf{A}_2 = \mu_0(2\mu_0 + \lambda) \mathbf{I}$ and

$$\mathcal{L}_1 = \begin{pmatrix} 0 & D_x \lambda_0 D_{\xi} + D_{\xi} \mu_0 D_x \\ D_{\xi} \lambda_0 D_x + D_x \mu_0 D_{\xi} & 0 \end{pmatrix}, \quad (13)$$

$$\mathbf{A}_0 = \begin{pmatrix} \mu_0 & 0 \\ 0 & \lambda_0 + 2\mu_0 \end{pmatrix}, \quad \mathbf{A}_1 = \begin{pmatrix} 0 & \mu_0 \\ \lambda_0 & 0 \end{pmatrix}. \quad (14)$$

Then, a part of the problem under consideration within the domain Ω_0 can be reformulated in the following manner: we should look for the solution \mathbf{w} in the domain Ω_0 satisfying the equation:

$$(\mathcal{L}_0 + \varepsilon \mathcal{L}_1 + \varepsilon^2 \mathcal{L}_2) \mathbf{w} = \mathbf{0}, \quad (x, \xi) \in \Omega_0, \quad (15)$$

and the interior transmission conditions:

$$\begin{aligned} \mathbf{u}_\pm(x, \pm \varepsilon h_0) &= \mathbf{w}(x, \pm h_0), \\ \sigma_\pm^{(y)}(x, \pm \varepsilon h_0) &= (\mathcal{M}_0 + \varepsilon \mathcal{M}_1) \mathbf{w}|_{\xi=\pm h_0}. \end{aligned} \quad (16)$$

According to a standard procedure [Movchan and Movhan (1995)], the solution within corresponding domains will be sought in form of asymptotic series:

$$\mathbf{w}(x, \xi) = \sum_{j=0}^{\infty} \varepsilon^j \mathbf{w}_j(x, \xi), \quad \mathbf{u}_\pm(x, y) = \sum_{j=0}^{\infty} \varepsilon^j \mathbf{u}_j^\pm(x, y). \quad (17)$$

As a result, sequence of the BVPs determining respective terms in asymptotic expansions (17) will be found. Thus, for the first term \mathbf{w}_0 , one can obtain:

$$D_\xi \mathbf{A}_0 D_\xi \mathbf{w}_0 = \mathbf{0}, \quad (x, \xi) \in \Omega_0, \quad (18)$$

$$\mathbf{u}_0^\pm(x, \pm 0) = \mathbf{w}_0(x, \pm h_0), \quad (19)$$

$$\sigma_{0\pm}^{(y)}(x, \pm 0) = \mathbf{A}_0 D_\xi \mathbf{w}_0|_{\xi=\pm h_0}. \quad (20)$$

From (18) and (20) one can immediately conclude that

$$\sigma_{0+}^{(y)}(x, +0) = \sigma_{0-}^{(y)}(x, -0), \quad (21)$$

while equation (18) is easily integrated to obtain:

$$\mathbf{w}_0(x, \xi) = \mathbf{u}_0^-(x, -0) + \int_{-h_0}^{\xi} \mathbf{A}_0^{-1}(x, t) dt \cdot \sigma_0^{(y)}(x, 0). \quad (22)$$

Finally, taking condition (19) into account, one can observe that an additional condition has to be satisfied for solvability of the problem (18) - (20):

$$\mathbf{u}_0^+(x, +0) - \mathbf{u}_0^-(x, -0) = \int_{-h_0}^{h_0} \mathbf{A}_0^{-1}(x, t) dt \cdot \sigma_0^{(y)}(x, 0). \quad (23)$$

Let us note that equations (21) and (23) constitute the sought for imperfect transmission conditions for the solutions u_0^\pm within the bonded materials. These transmission

conditions together with the boundary conditions (5)₁ allow us to find the solution of equations (1)₁ valid in the matched materials. Then, the main term of the solution within the interphase is simply calculated due to (22).

Continuing the procedure, one can obtain the solution within the whole domain with an arbitrary accuracy with respect to the small parameter ε . However, such solutions will still contain an error connected with the fact that the constructed solution does not satisfy boundary condition (5)₂.

In the case of the plane stress problem, all the results are still valid if λ is changed to $\lambda_* = 2\lambda\mu/(\lambda + 2\mu)$. This means that we have for plane strain problems :

$$\mu = \frac{E}{2(1+\nu)}, \quad \lambda = \frac{\nu E}{(1+\nu)(1-2\nu)}, \quad (24)$$

in case of plane stress problems, these parameters are defined as follows:

$$\mu_* = \frac{E}{2(1+\nu)}, \quad \lambda_* = \frac{\nu E}{1-\nu^2}, \quad 2\mu_* + \lambda_* = \frac{E}{1-\nu^2}. \quad (25)$$

Summarizing the obtained results, imperfect transmission conditions for the soft inhomogeneous interface can be written in the following manner:

$$[\sigma^{(y)}]|_{y=0} = \mathbf{0}, \quad [\mathbf{u}]|_{y=0} = \begin{pmatrix} \tau_1(x) & 0 \\ 0 & \tau_2(x) \end{pmatrix} \cdot \sigma_0^{(y)}(x, 0), \quad (26)$$

where the symbol $[f]|_S$ denotes the jump of a function f across an arbitrary boundary S , while new parameters are defined:

$$\tau_1(x) = \int_{-h_0}^{h_0} \frac{d\xi}{\mu_0(x, \xi)} = \int_{-h}^h \frac{dy}{\mu(x, y)}, \quad (27)$$

$$\tau_2(x) = \int_{-h}^h \frac{dy}{2\mu(x, y) + \lambda(x, y)}. \quad (28)$$

As it follows from Eq. (20), the main terms of the stress components σ_y, σ_{xy} are constants inside the interphase. Let us consider the last component σ_x :

$$\sigma_x = (2\mu + \lambda)\varepsilon_x + \lambda\varepsilon_y = \left[\varepsilon(2\mu_0 + \lambda_0) \frac{\partial}{\partial x}, \lambda_0 \frac{\partial}{\partial \xi} \right] \cdot \mathbf{w}(x, \xi).$$

The main term with respect to the small parameter ε is

$$\sigma_x(x, \xi) = \lambda_0 \frac{\partial}{\partial \xi} [0, 1] \cdot \mathbf{w}_0(x, \xi) + O(\varepsilon),$$

then taking into account Eq. (22), one can conclude:

$$\sigma_x(x, \xi) = \frac{\lambda_0}{2\mu_0 + \lambda_0} [0, 1] \cdot \sigma_0^{(y)}(x, 0) + O(\varepsilon),$$

or finally inside the interphase the last stress component varies in direction perpendicular to the interphase only if Poisson's ratio depends on the variable ξ :

$$\sigma_x(x, \xi) = \frac{\nu(x, \xi)}{1 - \nu(x, \xi)} \sigma_y(x, 0) + O(\varepsilon), \quad \varepsilon \rightarrow 0. \quad (29)$$

Thus, whereas the value of Young's modulus of the interphase depends on the variable ξ , the stress component σ_x does not depend on this variable because Poisson's ratio is constant.

Let us consider two particular cases of the transmission conditions. The first one appears when all the elastic parameters of the interphase are constant. Then, the interfacial parameters are also constants:

$$\tau_1 = \frac{4h(1 + \nu)}{E}, \quad \tau_2 = \frac{2(1 + \nu)(1 - 2\nu)h}{(1 - \nu)E} \quad (30)$$

for the plane strain and

$$\bar{\tau}_1 = \tau_1, \quad \bar{\tau}_2 = \frac{2(1 - \nu^2)h}{E} \quad (31)$$

for the plane stress case.

In the case when Poisson's ratio is a constant while Young's modulus of the interphase is a function of both variables, one can easily extract from (27) and (28) the same formulae as in (30) and (31), where the modulus E has to be only replaced by the auxiliary function:

$$\hat{E}(x) = \left(\int_{-h}^h \frac{dy}{E(x, y)} \right)^{-1}. \quad (32)$$

However, we have to mention in this place an essential difference between plane strain and plane stress problems. Namely, if the elastic intermediate phase is weakly compressible ($\nu = 0.5 - \varepsilon\nu_0$, $\nu_0 > 0$), then the condition $\mu \sim \lambda$ is not true (cf. (11)) in general. As a result, transmission conditions (26) are not justified for the weakly compressible interface in the case of plane strain problems [Mishuris (2004)].

One of the main questions, as it usually appears in asymptotic approaches, is: which magnitude of error will be introduced in the problem if one replaces the real thin

interphase by the evaluated imperfect transmission conditions. An additional problem which everywhere appears after formal asymptotic analysis is the estimation of regions where the asymptotic formulae give an acceptable result and where other methods (other conditions in this case) should be applied to correct the solution.

If one models the soft intermediate layer by the imperfect transmission conditions (26) then the relative error connected with such an approach can be estimated a priori from the asymptotic analysis in terms of $O(\varepsilon)$ except the regions near the intersections of the layer and the external boundary (Fig. 1). Nevertheless, it is impossible to estimate in value the ranges of the mentioned regions and the real error introduced in the solution.

One of the aims of this work is to provide numerical estimates for the aforementioned error as well as to clarify the sizes of the edge zone effects by FEM modelling of the thin intermediate layer in composite structures. We are not going to discuss here any questions concerning implementation of the imperfect transmission conditions in the numerical codes which is also an important problem to be solved.

3 FEM simulation

The commercial finite element code MSC.Marc is used for the simulation of the mechanical behavior of the thin intermediate layer with a dimension of $2h = H/100 = 0.01$ and $L = 10$. The two-dimensional FE-mesh is built up of four-node, isoparametric elements with bilinear interpolation functions. In order to investigate the edge effect (cf. Fig. 1, left and right hand side of the interphase), a strong mesh refinement is performed in this region. Furthermore, the mesh is generated in such a way that it is possible to evaluate the displacements and stresses along the axes of symmetry (cf. Fig. 2, lines A and B) and along the transition zone of the materials (cf. Fig. 2, lines C and D). In Fig. 2, the lines C^e and D^e belong to the bonded material and the lines Cⁱ and Dⁱ to the interphase. The MSC.Marc user subroutine feature is used to automatically derive the data along the above mentioned lines.

The final mesh and some details of the interphase with its strong mesh refinement are shown in Fig. 3. The whole mesh consists of 108544 Elements whereof 39512 Elements account for the interphase. The resulting

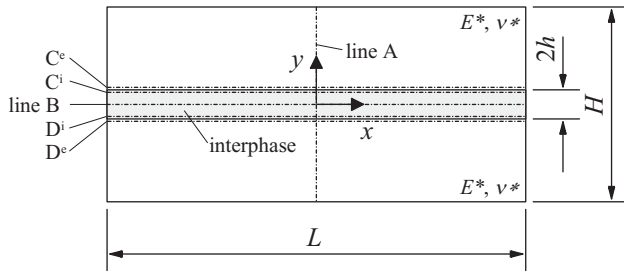


Figure 2 : Evaluation paths of the investigated structure

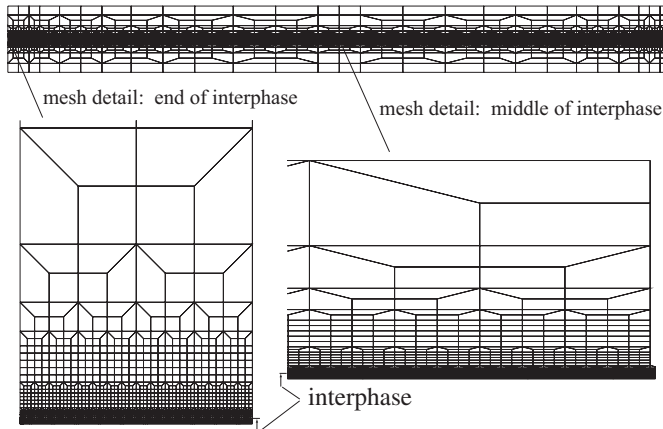


Figure 3 : Two-dimensional FE-mesh: strong mesh refinement in the investigated area

linear system of equations is still possible to solve in a short time on a standard personal computer with 1.5 GB RAM. Fig. 4 describes the mesh in more detail with the so-called mesh density (elements per length).

In the framework of the presented work, we investigate two load cases. In the so-called simple tensile case (cf. Fig. 5 a)), all nodes with $y = +H/2$ have a constant y -displacement and the x -displacement is constrained to zero. At the lower boundary ($y = -H/2$), all degrees of freedom are constrained to zero. In the so-called simple shear case (cf. Fig. 5 b)), the same fixed boundary is used at $y = -H/2$ and to all nodes with $y = +H/2$ a constant x -displacement is applied, whereas the y -displacement of these nodes is constrained to zero. Let us underline here that the simple shear case in our paper is not a pure shear state because bending is superimposed to the shear state due to the boundary conditions.

For these model calculations, the elastic constants, Young's modulus $E_{\pm} = E^* = 72700$ MPa and Poisson's ratio $\nu_{\pm} = \nu^* = 0.34$, of the aluminum alloy AlCuMg1

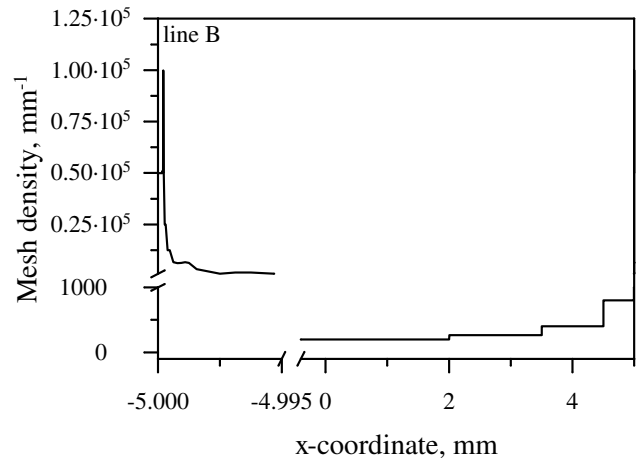
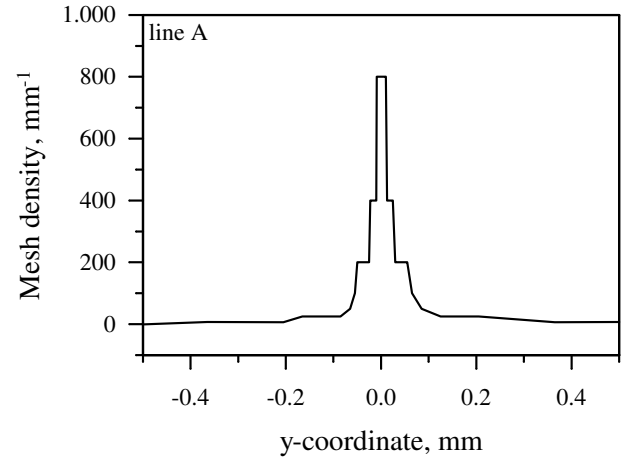


Figure 4 : Mesh density with reference to Fig. 2

(2017) are assigned to the bonded material (cf. Fig. 2). Differing elastic constants are chosen for the intermediate layer and the calculations are carried out for the plane stress and plane strain case.

We have restricted ourselves to the cases of the mentioned simple tensile and simple shear loading because the constructed FEM mesh is definitely appropriated for them. We have checked this fact by comparing the test results where $x = 0$ holds for the completely homogeneous elastic domain without intermediate zone ($E^* = E, \nu^* = \nu$) with two solutions. Theoretical solutions for simple tensile, shear and bending problems in rectangles can be found for example in [Flügge (1962)]. We also have compared those FEM solutions for our mesh with the FEM solutions for standard regular (without transition elements) mesh for the homogeneous elastic rectangle. As a result, we have made sure that for the tensile and shear loadings the constructed mesh with transition elements

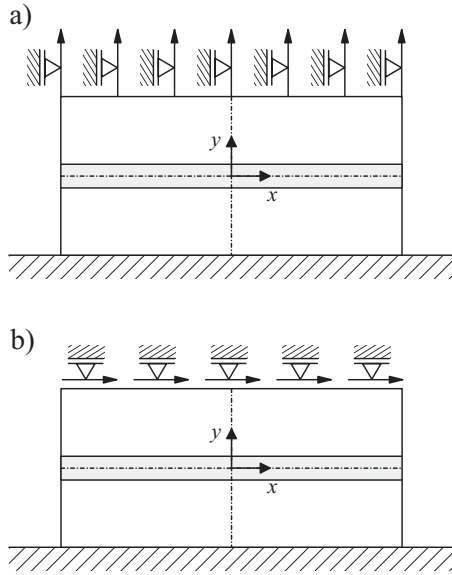


Figure 5 : Boundary conditions and loads: a) tensile case; b) shear case

works well, but not for the bending loading.

4 Numerical results and discussion

First of all let us note that, in the case when the elastic modulae of the intermediate layer are constant, equations (22) and (23) can be rewritten in the following form:

$$\mathbf{w}(x, \xi) = \mathbf{u}^-(x, -0) + (\xi + h_0) \mathbf{A}_0^{-1} \boldsymbol{\sigma}^{(y)}(x, 0), \quad (33)$$

$$[\mathbf{u}]_{y=0} = \begin{pmatrix} 2h/\mu & 0 \\ 0 & 2h/(2\mu + \lambda) \end{pmatrix} \boldsymbol{\sigma}^{(y)}(x, 0). \quad (34)$$

In the following, we will discuss the obtained numerical results in detail only for one case as an example: i.e. plane stress tensile loading with interface constants: $E = 813$ MPa, $\nu = 0.4999$. In Fig. 6, distributions of displacements and stresses along the line A (cf. Fig. 2) are presented. Note that the stress component $\sigma_x(0, y)$ is discontinuous at the interface boundaries, as it should be expected, while all other components are continuous. Although the ratio E/E^* can only be estimated as 0.1 while $2h/H = 0.01$, one can see that the distribution of the displacements within the interface exhibits linear character, which coincides with (33). Moreover, we can now check condition (34) at least at the point $x = 0$. For this reason, we calculate the difference between displacements $\Delta u_y = u_y^+ - u_y^-$ from different sides of the interface. In the first line of the table 2, the calculated value of $\Delta u_y/\sigma_y$

is presented whereas stress $\sigma_y = \sigma_y(0, 0)$ has been extracted directly from the subroutine (the different material combinations are explained in Tab. 1). This value can be compared, as it follows from (34), with the material constant $2h/(2\mu + \lambda)$. Although both values have an order of 10^{-7} , the relative error takes only a magnitude of 10^{-7} , which is essentially better than one can expect from the theoretical result where an estimate $O(\varepsilon^2)$ can be only justified ($\varepsilon^2 \sim 10^{-4}$). This fact can be probably explained in that way that next terms in the asymptotic expansions (17) disappear in this case, as an exception, due to the special symmetry of the loadings and geometry.

Note also that the value of $\Delta u_y(x)/\sigma_y(x)$ does not change practically along the entire interface, and the edge effect becomes essential only near the external boundary. To show this fact, distributions of the displacements and stresses along five lines B, Cⁱ, C^e, Dⁱ, D^e (cf. Fig. 2) are presented in Figs. 7 and 8 for the same example. The deviation between the lines of Fig. 7 at the free edge is not visible in the scale of the figure.

Let us note that the first component in the transmission condition (34) is satisfied identically for the entire interface as it follows from Figs. 7 and 8 due to tensile loading. In the case of the shear loading, the same results have been obtained for the second component of (34). These facts are simple consequences of the symmetry in geometrical and mechanical properties of the example under consideration. It is important to note that although the displacement is continuous along the interphase boundary, it is not smooth in y -direction and therefore, a visible difference of displacement for lines C^e, Cⁱ and D^e, Dⁱ can be observed in Fig. 7b. Furthermore, the decrease of σ_x at the free ends is not possible to observe in the given scale of Fig. 8 but indicated by the markers.

One can think that the displacements should behave in opposite way at the free edge in comparison with that presented in Figs. 7b and 8. At the first glance, the interphase stiffness seems to increase near the free edge, because the displacement decreases. In Fig. 9a, the final shape of the free edge boundary after the deformation is presented for the same sample with simple tensile loading. It is clear that such a behavior of the displacements near the free edge is reasonable because of the contraction. In order to compare two limiting cases of Poisson's ratio, the shape is drawn for the same tensile sample in Fig. 9b with another Poisson's ratio of $\nu = 0.0001$. Now,

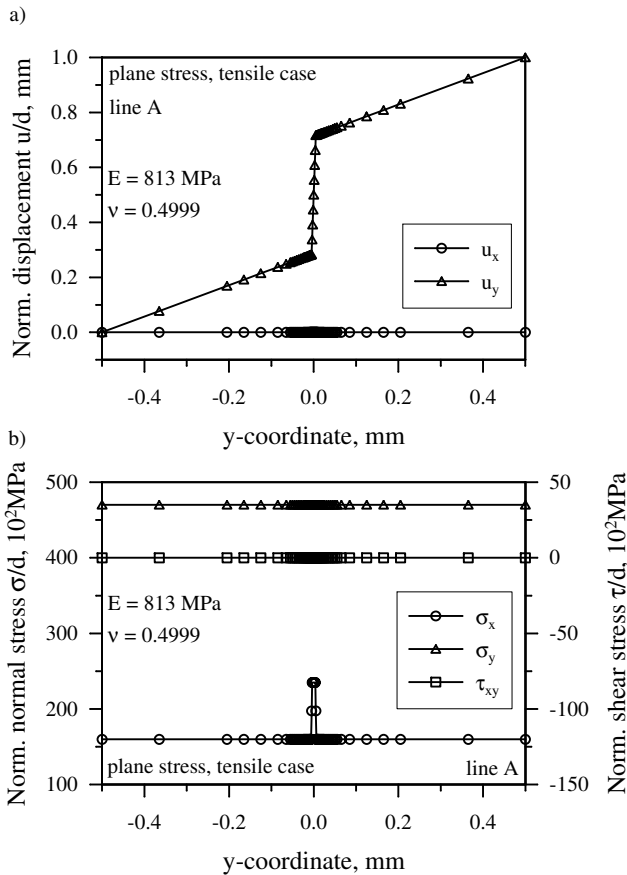


Figure 6 : Normalized displacement and stress distribution along line A (cf. Fig. 2)

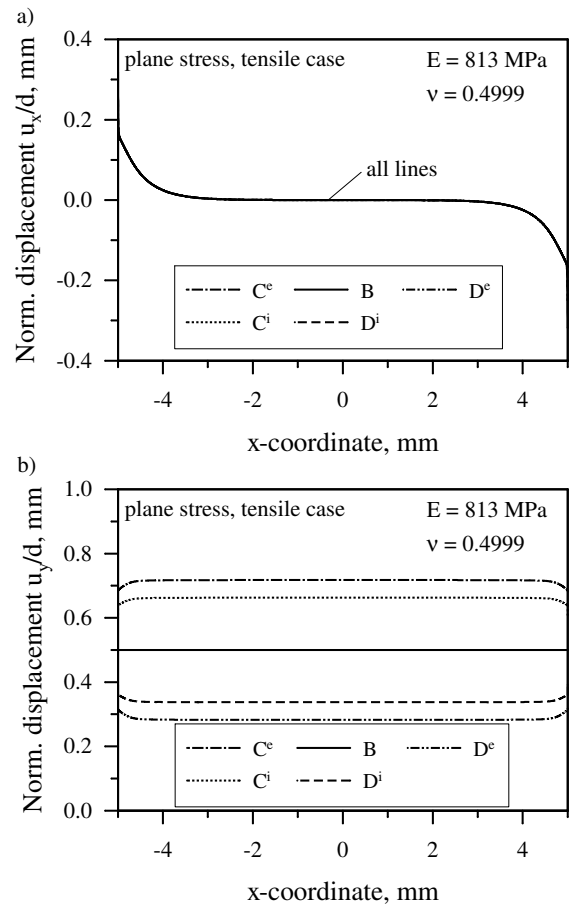


Figure 7 : Normalized displacement distribution along lines B, C and D (cf. Fig. 2)

there is practically no contraction of the interphase material. However, the distance from the free edge, measured where the stress component σ_y is no longer a straight line, is practically the same for both cases with an accuracy of 1% in the reference coordinate system.

In Tables 2-5 similar numerical results are presented for numerous combinations of the elastic constants, loadings and plane states. For the shear loading in plane strain, all results are practically the same as in the case of the simple shear loading in plane stress, which is evident from the problem formulation. To show this fact, we have presented only the first case for the weakly compressible interface in Table 5. Let us note that, in the case of the weakly compressible interface under plane strain conditions, the accuracy becomes to be essentially worse in comparison with all other cases under consideration. The explanation is quite simple. As we have mentioned earlier, the transmission conditions evaluated in the first sec-

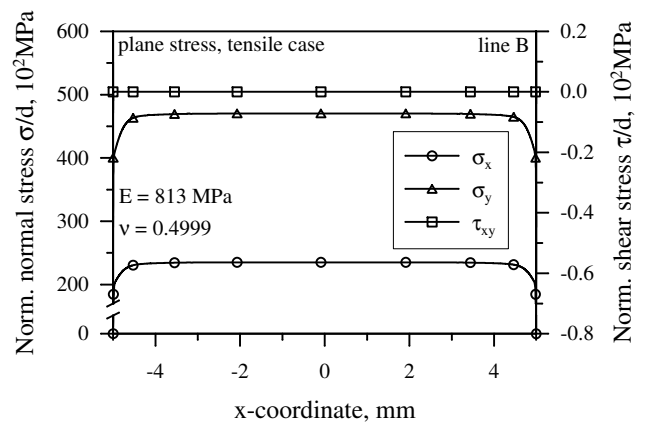


Figure 8 : Normalized normal and shear stress distribution along line B (cf. Fig. 2)

tion are no longer valid in such a case [Mishuris (2004)]. However, so-called locking phenomena also can occur in

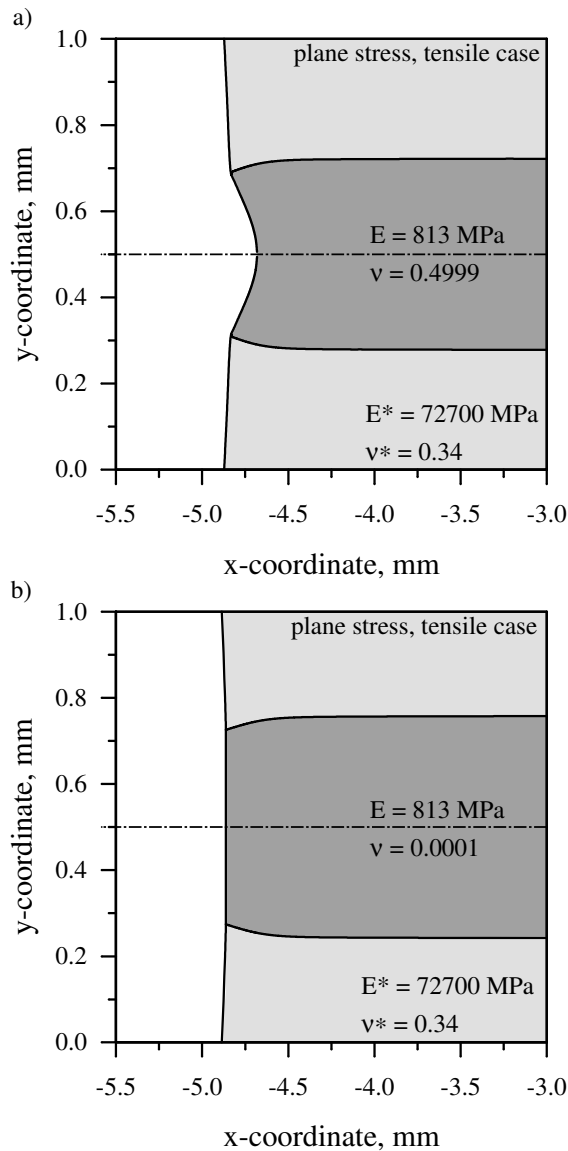


Figure 9 : Shape of the interphase near the free edge for different Poisson's ratios

this case and maybe also involved in the loss of numerical accuracy.

To our great surprise, the imperfect transmission conditions (34), being only justified for the soft thin interphase, are true for practically all examples on a sufficiently long distance along the interface from the center of the samples, as it follows from the tables. However, with increase of the ratio E/E^* , the region where this fact is observable becomes smaller.

The edge effect manifests its influence deeper within the sample. To estimate this influence we have introduced

the distance l from the ends of samples (Fig. 1) where the corresponding stress component measured along the interface becomes worse with an accuracy of 1% in comparison with the value at the symmetry axis. Let us note that it is possible to introduce alternative definitions of the edge effect zone based on the displacement components. It is a well known fact that the size of the zone depends on the definition, but the result is of the same order. Thus, the same definition is consequently used to provide the necessary information about the effect. We use everywhere the parameter $\delta = 2l/L$ showing the relative deepness of this zone. This edge effect is connected with Saint-Venant's principle. In fact, in the case of the infinite strip one can easily show that the stress will be constant along the interface. Thus, the observed changing of the behavior near the sample edges in Fig. 8 is due to the boundary conditions applied to the edges (in this paper: free edge). The main tendency concerning the edge effect may essentially differ for other boundary conditions in comparison with the discussed one.

Table 1 : Investigated material cases (MC)

MC	E	ν
1	8138	0.4999
2	813	0.4999
3	81	0.4999
4	5427	0.0001
5	542	0.0001
6	54	0.0001
7	8138	0.3000
8	813	0.3000
9	81	0.3000
10	271270	0.3000

In Figs. 10-12, corresponding values of δ are presented for different cases under consideration. Except the case of the weakly compressible interface ($\nu = 0.4999$) under plane strain conditions for tensile loading, all curves in Figs. 10-12 $\delta = \delta(E/E^*)$ exhibit a similar behavior. Namely, for small values of the ratio $E/E^* \sim 10^{-3}$, δ takes a value near 0.05 and for smaller values (see Fig. 12) it becomes comparable with the accuracy of δ due to the definition. Moreover, the magnitude of Poisson's ratio slightly influences the value of δ , except the mentioned case of the weakly compressible interface under plane strain conditions and tensile loading.

Table 2 : Plane stress, tensile case, line A

MC	$\frac{\Delta u_y(0,0)}{\sigma_y(0,0)}$	$\frac{2h(1-\nu^2)}{E}$	rel. error
1	$9.2173 \cdot 10^{-7}$	$9.2173 \cdot 10^{-7}$	$1.085 \cdot 10^{-7}$
2	$9.2264 \cdot 10^{-6}$	$9.2263 \cdot 10^{-6}$	$3.577 \cdot 10^{-6}$
3	$9.2605 \cdot 10^{-5}$	$9.2605 \cdot 10^{-5}$	$9.719 \cdot 10^{-7}$
4	$1.8426 \cdot 10^{-6}$	$1.8426 \cdot 10^{-6}$	$-1.085 \cdot 10^{-6}$
5	$1.8450 \cdot 10^{-5}$	$1.8450 \cdot 10^{-5}$	$1.626 \cdot 10^{-6}$
6	$1.8519 \cdot 10^{-4}$	$1.8519 \cdot 10^{-4}$	$1.080 \cdot 10^{-6}$
7	$1.1182 \cdot 10^{-6}$	$1.1182 \cdot 10^{-6}$	$8.943 \cdot 10^{-6}$
8	$1.1193 \cdot 10^{-5}$	$1.1193 \cdot 10^{-5}$	$2.680 \cdot 10^{-6}$
9	$1.1235 \cdot 10^{-4}$	$1.1235 \cdot 10^{-4}$	$8.901 \cdot 10^{-7}$
10	$3.3550 \cdot 10^{-8}$	$3.3546 \cdot 10^{-8}$	$1.264 \cdot 10^{-4}$

Table 3 : Plane strain, tensile case, line A

MC	$\frac{\Delta u_y(0,0)}{\sigma_y(0,0)}$	$\frac{2h(1+\nu)(1-2\nu)}{E(1-\nu)}$	rel. error
1	$7.7872 \cdot 10^{-10}$	$7.3709 \cdot 10^{-10}$	0.0565
2	$7.4210 \cdot 10^{-9}$	$7.3781 \cdot 10^{-9}$	0.0058
3	$7.3850 \cdot 10^{-8}$	$7.4054 \cdot 10^{-8}$	-0.0028
4	$1.8426 \cdot 10^{-6}$	$1.8426 \cdot 10^{-6}$	$4.342 \cdot 10^{-6}$
7	$9.1285 \cdot 10^{-7}$	$9.1283 \cdot 10^{-7}$	$3.177 \cdot 10^{-5}$

Table 4 : Plane stress, shear case, line A

MC	$\frac{\Delta u_x(0,0)}{\sigma_{xy}(0,0)}$	$\frac{4h(1+\nu)}{E}$	rel. error
1	$3.6862 \cdot 10^{-6}$	$3.6862 \cdot 10^{-6}$	$-1.899 \cdot 10^{-6}$
2	$3.6898 \cdot 10^{-5}$	$3.6898 \cdot 10^{-5}$	$1.084 \cdot 10^{-6}$
3	$3.7035 \cdot 10^{-4}$	$3.7035 \cdot 10^{-4}$	$7.020 \cdot 10^{-6}$
4	$3.6856 \cdot 10^{-6}$	$3.6856 \cdot 10^{-6}$	$-5.155 \cdot 10^{-6}$
5	$3.6904 \cdot 10^{-5}$	$3.6904 \cdot 10^{-5}$	$1.074 \cdot 10^{-7}$
6	$3.7041 \cdot 10^{-4}$	$3.7041 \cdot 10^{-4}$	$-4.050 \cdot 10^{-6}$
10	$9.5851 \cdot 10^{-8}$	$9.5845 \cdot 10^{-8}$	$5.842 \cdot 10^{-5}$

Table 5 : Plane strain, shear case, line A

MC	$\frac{\Delta u_x(0,0)}{\sigma_{xy}(0,0)}$	$\frac{4h(1+\nu)}{E}$	rel. error
1	$3.6860 \cdot 10^{-6}$	$3.6862 \cdot 10^{-6}$	$5.154 \cdot 10^{-5}$

This phenomenon shows that the edge effect zone is not only connected with the edge boundary conditions but also with properties of the bimaterial strip. Such a behavior can be easily explained. In fact, when the ratio of Young's modulus E/E^* tends to zero, one can expect that the top part of the strip will move as a rigid body

(without any traction applied from the absolutely weak interface). Alternatively, in the case of the other limiting case - strong stiff interface, the interface will move as a rigid straight line parallel itself and two different problems for the strips of the thickness h appear under total deformation $U/2$ of each strip. Then, it is clear that such a case should be equivalent, with respect to the edge zone analysis, with the homogeneous strip of the thickness $2h$ and total deformation U . However, because of the problem linearity, the edge zone should be of the same order. This means that with increasing ratio E/E^* the length of the edge zone has a tendency to stabilize near some plateau as it is easy to observe from all presented graphs in Figs 10 - 12. Moreover, one can easily realize that in the case of the weakly compressible interface two bonded half-strip are connected by this interface which still transmits forces from one part to another.

On the other hand, $\delta = 0.05$ means that $l = 50h$, so that the depth of the edge zone is 25 times longer than the thickness of the interphase.

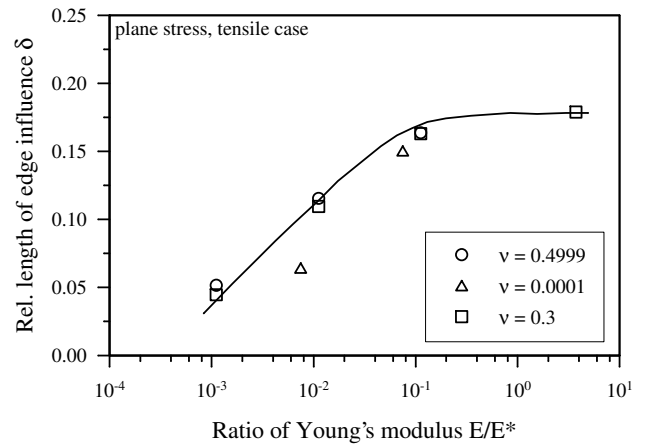


Figure 10 : Relative length of edge influence δ for plane stress tensile case

Finally, we would like to check the validity of the transmission condition in the case of the soft nonhomogeneous interface. For this reason we choose as an example a parabolic behavior of the interphase Young's modulus in the form $E(y) = 696.86(1 + 22680.0y^2)$, while Poisson's ratio remains constant $\nu = 0.4999$. As a result, the auxiliary parameter \hat{E} defined in (32) takes the same value $\hat{E} = 813.0$ as discussed in one of the homogeneous cases under consideration.

In Fig. 13, distributions of the displacements and stresses

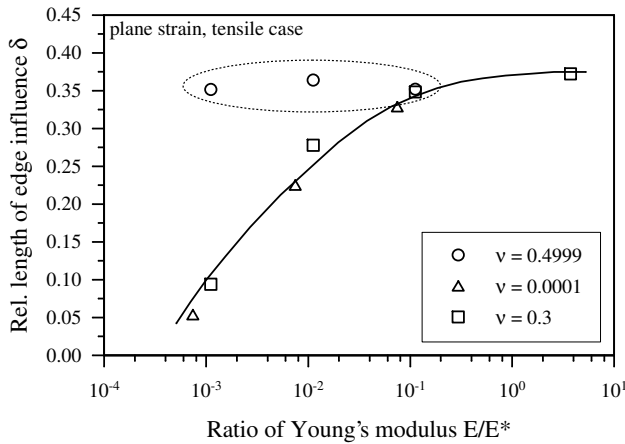


Figure 11 : Relative length of edge influence δ for plane strain tensile case

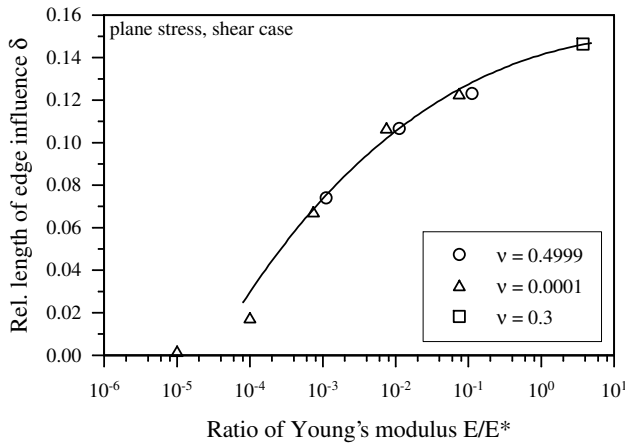


Figure 12 : Relative length of edge influence δ for plane stress shear case

in perpendicular direction to the interface at the symmetry line $x = 0$ are presented. The only difference between the graphs in Fig. 6b and Fig. 13b is the scaling. We do not present such magnification earlier in of Fig. 6 where the stresses took practically constant values within the interface (with accuracy more than 0.01%, which, in fact, is better than it has been predicted by the asymptotic analysis). This is no more valid with the same accuracy for the nonhomogeneous interphase. It is clear from Fig. 13b that in the case under consideration the stresses within the interface differ now about 2.4% in the worst point from the constant behavior.

However, it is important to note that the increase of the gradient in the definition of Young's modulus leads to a loss of accuracy in the calculation. This behavior is

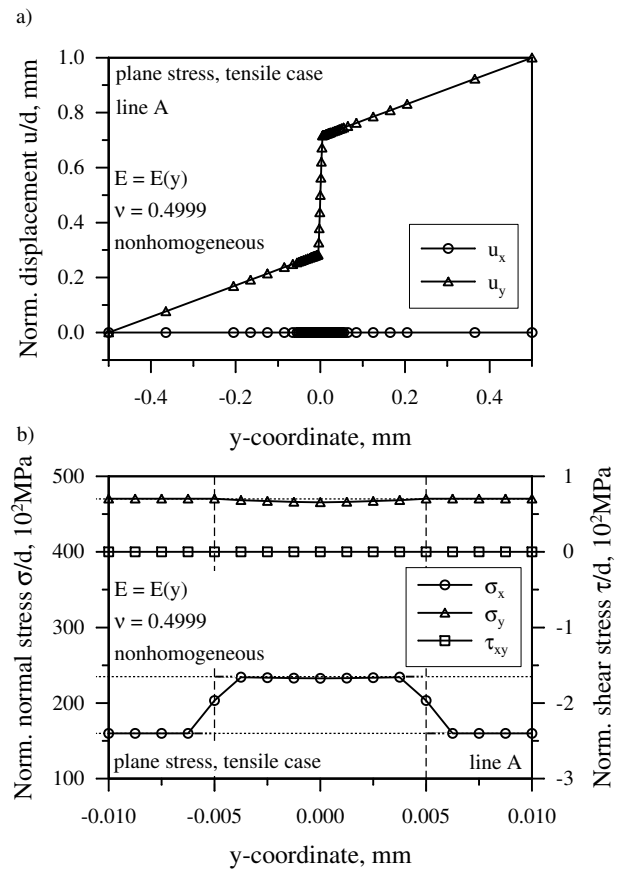


Figure 13 : Normalized displacement and stress distribution along line A (cf. Fig. 2)

connected with the small amount of nodes in direction perpendicular to the interphase used in the constructed mesh (only 9 nodes within the interface in perpendicular direction). Let us also note that the stress component σ_x is a constant within and outside the interphase ($|y| < h$) and has a jump at the interface lines ($y = \pm h$). However, this jump is not well approximated due to the few finite elements in that region. Of course, one can easily draw the right behavior.

On the other hand, when we decrease the gradient in the material properties of the interphase, the stress inside the interphase becomes again to be constant. However, even with the chosen sufficiently large change in material properties within the interphase, the accuracy of the transmission conditions is still very high.

To clarify this, two terms which are involved in one of the imperfect transmission conditions, i.e. Δu_y and $\tau_1 \sigma_y(x, 0)$, are presented in Fig. 14. The other condition

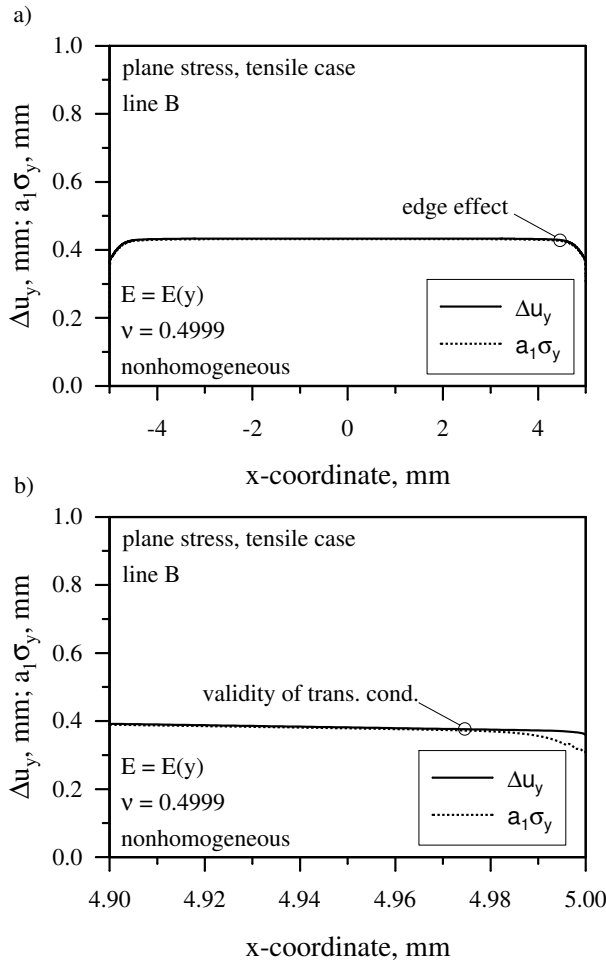


Figure 14 : Determination of the edge effect and the validity of the transmission conditions for a nonhomogeneous interphase (with the normalization $d = 1$)

is a priori satisfied due to the problem symmetry. As one can see no difference between the functions can be observed. The edge effect zone can be determined for the simple tensile loading by defining 1% accuracy of the values of both functions from that at the symmetry point $x = 0$. On the other hand, one can also observe that the transmission conditions are still valid within the edge effect zone! To show this fact, a magnification of the graph is presented near the right hand side of the free edge. It is known from the asymptotic analysis that the evaluated transmission conditions cannot be valid along the whole interface up to the very end. However, as it follows from the figure, the region where they fail is extremely smaller than the edge effect zone itself.

5 Conclusion and further work

As it follows from the presented numerical results, imperfect transmission conditions for the soft interphase (34) obtained analytically by asymptotic analysis is satisfactory with a very good accuracy even in the case $\epsilon = 0.01$.

The edge effect appears only on a distance comparable with twenty five times the thickness of the interface in the case of the soft interface and it even decreases when E/E^* becomes smaller. However, the zone increases essentially with increasing ratio E/E^* approaching some limiting value. However, the transmission conditions are still valid within the edge effect zone and they fail only near the singularity dominated domain which is extremely small.

In the second part of this paper, we are going to consider asymmetric cases, i.e. different bonded materials, to verify whether a so high accuracy of the imperfect transmission conditions in comparison with the theoretical prediction is connected with the problem symmetry. Also we are planning to check other transmission conditions valid for stiff interfaces. Among others, a range of its applicability and boundary layer effects will be investigated. Finally, we are going to analyze a phenomenon connected with the singularity dominated regions (possible stress singularity near the singular points - intersections of the interface and the external boundary).

Although FEM analysis is very useful for verification in value of formal asymptotic analysis, it has its own restrictions concerning values of the small parameter and strong difficulties connecting with necessity to build a complicated mesh which can be additionally depending on the type of loading, as it occurred in our investigations for bending. It is also difficult to define an unknown form of corresponding transmission conditions from the FEM analysis. However, in the case when one can suppose any specific conditions, they can be numerically verified. In such a way there is a possibility to evaluate imperfect transmission conditions in the case when respective asymptotic analysis is difficult to be carried out. Taking this fact into account, we are going to evaluate and verify transmission conditions for thin plastic interphases.

Acknowledgement: A. Öchsner is grateful to Portuguese Foundation of Science and Technology for financial support. G. Mishuris is grateful to EU Marie Curie

grant MTKD-CT-2004-509809.

References

Allen, H.G. (1969): *Analysis and Design of Structural Sandwich Panels*, Pergamon Press, Oxford.

Antipov, Y.A.; Avila-Pozos, O.; Kolaczowski, S.T.; Movchan, A.B. (2001): Mathematical model of delamination cracks on imperfect interfaces, *Int J Solids Struct*, vol. 38, pp. 6665-6697.

Ashby, M.F.; Evans, A.; Fleck, N.A.; Gibson, L.J.; Hutchinson, J.W.; Wadley, H.N.G. (2000): *Metal Foams: A Design Guide*, Butterworth-Heinemann, Boston.

Flügge, W. (1962): *Handbook of Engineering Mechanics*, McGraw-Hill Book Company, New York.

Hatheway, A.E. (1989): Evaluating Stresses in Adhesive Bond Lines. In: *Proc. MSC/NASTRAN Users' Conference*, Universal City.

Mishuris, G. (2004): Imperfect transmission conditions for a thin weakly compressible interface. 2D problems. *Arch Mech*, vol. 56, pp. 143-154.

Mishuris, G.; Kuhn, G. (2001): Asymptotic Behaviour of the Elastic Solution near the Tip of a Crack Situated at a Nonideal Interface. *ZAMM*, vol. 81, pp. 811-826.

Movchan A.B.; Movhan, N.V. (1995): *Mathematical Modelling of Solids with Nonregular Boundaries*, CRC Press, Boca Raton.

Pradhan, S.C.; Lam, K.Y.; Tay, T.E. (2000): Determination of Fracture Parameters of Laminated Thermoplastic Composite Materials: A Finite Element Approach. *Int J Adhes*, vol. 50, pp. 395-401.